Multiple Replacements of Glutamine 143 in Human Manganese Superoxide Dismutase: Effects on Structure, Stability, and Catalysis[†]

Vincent J.-P. Lévêque,[‡] M. Elizabeth Stroupe,[§] James R. Lepock,[∥] Diane E. Cabelli,[⊥] John A. Tainer,[§] Harry S. Nick,[#] and David N. Silverman*,[▽]

Departments of Pharmacology, Biochemistry, and Neuroscience, University of Florida, Gainesville, Florida 32610, Department of Molecular Biology, The Scripps Research Institute, 10550 North Torrey Pines Road, La Jolla, California 92037, Department of Physics, University of Waterloo, Waterloo, Ontario N2L3G1, Canada, and Department of Chemistry, Brookhaven National Laboratory, Upton, New York 11973-5000

Received December 30, 1999; Revised Manuscript Received March 31, 2000

ABSTRACT: Glutamine 143 in human manganese superoxide dismutase (MnSOD) forms a hydrogen bond with the manganese-bound solvent molecule and is investigated by replacement using site-specific mutagenesis. Crystal structures showed that the replacement of Gln 143 with Ala made no significant change in the overall structure of the mutant enzyme. Two new water molecules in Q143A MnSOD were situated in positions nearly identical with the Oϵ1 and Nϵ2 of the replaced Gln 143 side chain and maintained a hydrogen-bonded network connecting the manganese-bound solvent molecule to other residues in the active site. However, their presence could not sustain the stability and activity of the enzyme; the main unfolding transition of Q143A was decreased 16 °C and its catalysis decreased 250-fold to $k_{cat}/K_m = 3 \times 10^6$ M^{-1} s^{-1}, as determined by stopped-flow spectrophotometry and pulse radiolysis. The mutant Q143A MnSOD and other mutants at position 143 showed very low levels of product inhibition and favored Mn(II)SOD in the resting state, whereas the wild type showed strong product inhibition and favored Mn(III)SOD. However, these differences did not affect the rate constant for dissociation of the product-inhibited complex in Q143A MnSOD which was determined from a characteristic absorbance at 420 nm and was comparable in magnitude ($\sim$100 s^{-1}) to that of the wild-type enzyme. Hence, Gln 143, which is necessary for maximal activity in superoxide dismutation, appears to have no role in stabilization and dissociation of the product-inhibited complex.

The manganese superoxide dismutases function through sequential redox processes in which the metal cycles between oxidized and reduced states.

$$\text{P-Mn}^{3+} + \text{O}_2^{\cdot-} \underset{k_{-1}}{\overset{k_1}{\rightleftharpoons}} [\text{P-Mn}^{3+}\text{-O}_2^{\cdot-}] \overset{k_2}{\rightleftharpoons} \text{P-Mn}^{2+} + \text{O}_2 \quad (1)$$

$$\text{P-Mn}^{2+} + \text{O}_2^{\cdot-} + 2\text{H}^+ \underset{k_{-3}}{\overset{k_3}{\rightleftharpoons}} [\text{P-Mn}^{2+}\text{-O}_2^{\cdot-}] + 2\text{H}^+ \overset{k_4}{\rightleftharpoons} \text{P-Mn}^{3+} + \text{H}_2\text{O}_2 \quad (2)$$

$$\text{P-Mn}^{3+}\text{-X} \quad (k_5 \downarrow\uparrow k_{-5})$$

Here P−Mn^{3+} represents the manganese bound in the enzyme. Catalysis by human manganese superoxide dismutase (MnSOD)[1] (*1*) and MnSOD from *Thermus thermophilus* (*2*) measured by stopped-flow spectrophotometry and pulse radiolysis show an efficient enzyme with a turnover number k_{cat} near 10^4 s^{-1} and k_{cat}/K_m near diffusion control. Initial studies of MnSOD from *Bacillus stearothermophilus* determined that its catalysis is complicated by the presence of a phase zero-order in superoxide, indicating an inactive form of the enzyme that can interconvert to an active form (*3*). Bull et al. (*2*) observed the inactive form spectrophotometrically at many wavelengths during the steady state and suggested that it is a form of product inhibition resulting from oxidative addition of $O_2^{\bullet-}$ to Mn(II)SOD, likely giving a side-on peroxo complex of Mn(III)SOD. This inhibited state is represented by P−Mn^{3+}−X in eq 2.

Human MnSOD is a homotetramer of four 22 kDa subunits; one manganese atom is bound between the α-helical domain and the α/β domain of each monomer, as shown in Figure 1A. The crystal structure shows the manganese bound in a trigonal bipyramidal coordination with three histidine ligands, one monodentate aspartate, and one manganese-bound water (or hydroxide) (*4*). Five residues near the manganese that do not directly coordinate the metal have been found by site-directed mutagenesis to influence the rate of catalysis; they are His 30 (*5*, *6*), Tyr 34 (*7*−*10*), Gln 143 (*11*), Trp 161 (*12*), and Tyr 166 (*6*). Of these five sites, amino acid replacement at position 143 has the largest

[†] This work was supported by National Institutes of Health Grants GM54903 (to D.N.S.), GM48495 (to J.A.T.), and HL39593 (to H.S.N.).

* Address correspondence to this author at Box 100267, Health Center, University of Florida, Gainesville, FL 32610-0267. Phone: (352) 392-3556, Fax: (352) 392-9696, E-mail: silvrmn@nervm.nerdc.ufl.edu.

[‡] Department of Biochemistry, University of Florida.

[§] Department of Molecular Biology, The Scripps Research Institute.

[∥] Department of Physics, University of Waterloo.

[⊥] Department of Chemistry, Brookhaven National Laboratory.

[#] Department of Neuroscience, University of Florida.

[▽] Department of Pharmacology, University of Florida.

[1] Abbreviations: MnSOD, manganese superoxide dismutase; Caps, 3-(cyclohexylamino)propanesulfonic acid; Ches, 2-(cyclohexylamino)-ethanesulfonic acid; Mops, 3-(*N*-morpholino)propanesulfonic acid; Taps, 3-[tris(hydroxymethyl)methyl]aminopropanesulfonic acid.

10.1021/bi9929958 CCC: $19.00
Published on Web 05/20/2000

effect on catalytic activity. The amide of the side chain of Gln 143 forms a hydrogen bond with the manganese-bound water and also with the hydroxyl side chain of Tyr 34. These residues form a hydrogen-bonded network that includes other water molecules and extends to other residues in the active-site cavity. Replacing Gln 143 with Asn caused a decrease of 2−3 orders of magnitude in catalytic activity compared with wild type, and caused an increase in the redox potential of the metal, resulting in an enzyme that favored the Mn(II)SOD in the resting state. Moreover, the mutant Q143N MnSOD was reported to have no significant product inhibition (*11*).

We investigated position 143 of human MnSOD with further amino acid replacements to determine if we could generate appreciable catalytic activity while maintaining a condition of low product inhibition. The crystal structure of the mutant containing the replacement of Gln 143 with Ala showed that two new water molecules were situated in positions nearly identical with the Oϵ1 and Nϵ2 of the replaced Gln 143 side chain. These water molecules maintained a hydrogen-bonded network in the active-site cavity; however, their presence could not sustain the stability and activity of the enzyme. Each of the five replacements we made at position 143 decreased catalytic activity 2−3 orders of magnitude compared with the activity of the wild type but also showed an optical spectrum during catalysis with an absorbance at 420 nm which is evidence of the product-inhibited state (*2*, *13*). Measurement of the decay of this absorbance suggests that the dissociation of the product-inhibited complex is not affected by the replacement Gln 143 → Ala. Hence, the features of the active site that influence catalysis appear to be different from the features that influence dissociation of the product-inhibited complex for these enzymes. This information is significant in designing mutants of MnSOD for gene therapy research that show less product inhibition than wild type and maintain a high level of catalytic activity.

MATERIALS AND METHODS

Mutagenesis and Expression. The oligonucleotides GCATATGAAGCACAGCCTCC and GGAGATCTCAGCATAACGATC were used as primers for PCR to amplify the human MnSOD cDNA [cDNA sequence reported by Beck et al. (*14*)]. The plasmid pHMNSOD4 (ATCC 59947) which contains human MnSOD was subcloned into the TA cloning vector pCRII (Invitrogen Corp.). A series of primers were designed to create the mutants Q143X in human MnSOD (X = A, E, H, N, S, V). First, we designed a pair of oligonucleotides, primers 1 (5′-C GCT AGT AAT CAT TTC ATG AAG CAC AGC CTC CCC G-3′) and 2 (5′-CGC CAA AAC AGC CAA GCT TTC ATG CTC GCA G-3′), which, through PCR, would recreate the entire MnSOD coding region. Second, we prepared two oligonucleotides for each mutant to be made, designated as primers 3 (5′-GCT GCT TGT CCA AAT CAG GAT CCA C-3′) and 4 (5′-G TGG ATC CTG ATT TGG ACA AGC AGC-3′), whose sequences are complementary to each other and contain the mutation of interest at position 143 (underlined). Two separate PCR reactions were used to amplify the 5′ half (primers 1 and 4) and 3′ half (primers 3 and 2) of the MnSOD cDNA coding sequence. The PCR products from these two reactions were purified using electroelution and used as template DNA for the second round of PCR using primers 1 and 2. The Q143X MnSOD PCR products were cloned into the expression vector p*Trc* 99A (Pharmacia Corp.). Cloning was accomplished by using the restriction sites *Bsp*HI and *Pst*I incorporated into primers 1 and 2, respectively. The *Bsp*HI site, which corresponds to the N-terminal portion of the protein, was annealed to the compatible cohesive ends of the *Nco*I site in p*Trc* 99A, recreating an ATG codon. The C-terminal end of the cDNA was cleaved and annealed to p*Trc* 99A using *Pst*I. The mutation was verified by DNA sequencing, along with the remainder of the coding sequence. This construct expressed human MnSOD as a mature protein in the mutant *Sod A*$^-$*/Sod B*$^-$ *E. coli* (strain QC 774), and tagged with an extra methionine at the amino terminus. Culture conditions included 660 μM $MnCl_2$. Yields were on average 70 mg of mutant MnSOD protein per 50 g of bacterial pellet.

Purification. Mutants of human MnSOD were purified from *E. coli* using a combination of heat treatment (60 °C), dialysis, and ion exchange chromatography (DE52 and CM52) according to the procedures of Beck et al. (*15*). The purity of the resulting samples was determined on SDS−polyacrylamide gels which showed one intense band. Each mutant was dialyzed thoroughly against EDTA and then analyzed for manganese content by atomic absorption spectroscopy. These measurements were used to determine the concentration of active enzyme on a monomeric basis. In all of our calculations of purified enzyme, the concentration of enzyme is taken as the manganese concentration determined by atomic absorption spectroscopy. The fraction of active sites occupied by manganese was determined to vary from 0.44 for Q143E to 0.75 for Q143S. Protein concentrations were determined by the Lowry method.

Crystallography of Q143A MnSOD. The hexagonal crystals of Q143A MnSOD were grown out of 2.0−2.8 M ammonium sulfate and 100 mM imidazole/malate buffer at pH 7.5 or 8.0. The data were collected at the Stanford Synchrotron Radiation Laboratory (beam-line 9-1) from a single crystal that was frozen in its well solution containing 20% ethylene glycol. The structure was solved by molecular replacement using the AMoRe program from the hexagonal Y34F human MnSOD mutant (*10*), and the proper residues were changed using XFIT (*16*). The crystals were in space group *p6(1)22* with a dimer in the asymmetric unit and the tetramer formed across a crystallographic 2-fold axis. The unit cell was 79.6 Å × 79.6 Å × 241.6 Å with angles of 90°, 90°, and 120° for α, β, and γ, respectively. Based on the absorbance at 480 nm, the Mn was considered to be primarily reduced and was treated formally as Mn(II). The Mn-bound solvent molecule was treated as a neutral water molecule. The ligand-to-metal distances were not constrained during refinement, except to specify that they were covalently bonded in order to avoid van der Waals interactions between the residues and the metal.

The following statistics apply to the refinement: resolution range, 20.0−2.12 Å; R_{free}, 26.49%; $R_{working}$, 22.99%; overall *B*-factor, 22.0 Å^2; total number of reflections, 89 153; total number of unique reflections, 26 135; number of reflections in the test set, 2574 (9.6%); percent completeness, 97.9%; R_{symm}, 7.7%; R_{symm} in the highest resolution bin, 33.2%; I/σ, 15.0; I/σ in the highest resolution bin, 3.32; mosaicity, 0.406. Atomic coordinates have been deposited in the Protein Data Bank with accession codes 1EM1 and RCSB010714.

Differential Scanning Calorimetry. A NANO high-sensitivity differential scanning calorimeter (Calorimetry Science Corp.) was used to obtain all denaturation profiles. Human MnSOD mutants were scanned at a concentration of 1.0 mg/mL (DSC cell volume is 0.8909 mL) in 20 mM potassium phosphate buffer (pH 7.8); samples were deaerated under mild vacuum for 5 min and immediately scanned at a rate of temperature increase of 1 °C/min. The baseline and change in specific heat (C_p) upon denaturation were corrected as previously described (*17*). The peaks of the differential scanning calorimetry profile were fit assuming a reversible, non-two-state model (*18*) using the software package ORIGIN (Microcal, Inc.) to obtain the enthalpy (ΔH) and entropy (ΔS) values. The temperature of half-completion (T_m) for each transition was obtained from the integral for each curve.

Stopped-Flow Spectrophotometry. Experiments are based on the stabilization of KO_2 in aprotic solvent and the subsequent large dilution of this solution by an aqueous solution of enzyme in a stopped-flow apparatus, as described by McClune and Fee (*19*). KO_2 was dissolved in dimethyl sulfoxide (DMSO) with the solubility of KO_2 enhanced with 18-crown-6 ether (*20*). Steady-state kinetic constants for the catalysis were determined at a single wavelength (the absorption of $O_2^{\bullet-}$ at 250−260 nm) with a stopped-flow spectrophotometer (Kinetic Instruments, Ann Arbor, MI). This instrument was capable of efficient mixing of superoxide in DMSO with an aqueous solution of enzyme in buffer (dead time between 1.5 and 2.0 ms). One drive syringe (capacity 50 μL) contained the aprotic solution of $O_2^{\bullet-}$; this was diluted 50-fold by the contents of a second syringe (capacity 2.5 mL) which contained enzyme, EDTA, and buffer. The decay of superoxide in initial velocity experiments (the first 5−10% of reaction) and progress curves were monitored by the absorption of $O_2^{\bullet-}$ at 260 nm ($\epsilon_{250} = 2000$ M^{-1} cm^{-1}). The range of concentrations of superoxide was from 20 μM to 1.0 mM. Stopped-flow experiments reported here were carried out at 20 °C. Eight kinetic traces were averaged to reduce noise. Steady-state parameters were obtained by least-squares analysis of such data (Enzfitter, Biosoft, Cambridge, U.K.).

Experiments were also performed using scanning stopped-flow spectrophotometry (SX18.MV; Applied Photophysics, Ltd., U.K.). We used a procedure of sequential mixing. First, a solution of $O_2^{\bullet-}$ in DMSO (described above) was mixed at a 1:3.5 ratio with an aqueous solution of 2 mM Caps and 1 mM EDTA at pH 11. At this pH, superoxide is considerably stabilized in its uncatalyzed dismutation (*21*). This solution was aged 1 s and then mixed in a 1:1 ratio with an aqueous solution of 300 mM Ches at pH 9.0. Absorbance spectra after mixing were measured at a rate of 400 spectra per second.

Pulse Radiolysis. Experiments were carried out using the 2 MeV van de Graaff accelerator at Brookhaven National Laboratory. Dosimetry was established using the KSCN dosimeter, assuming that $(SCN)_2^-$ has a G value of 6.13 and a molar absorptivity of 7950 M^{-1} cm^{-1} at 472 nm. All UV/Vis spectra were recorded on a Cary 210 spectrophotometer thermostated at 25 °C. The path length was either 2.0 or 6.1 cm. Solutions contained enzyme, 30 mM sodium formate [as a hydroxyl radical scavenger (*22*)], 50 μM EDTA, and 2 mM samples of one of the following buffers: Mops (pH 7.2), Taps (pH 8.2), and Ches (pH 9.2). Superoxide radicals were generated upon pulse radiolysis of an aqueous, air/O_2-saturated solution containing sodium formate according to the mechanisms described by Schwarz (*22*). Under our conditions, the formation of $O_2^{\bullet-}$ radicals is more than 90% complete by the first microsecond after the pulse. Changes in the absorbance of superoxide or enzyme were observed spectrophotometrically.

Table 1: Active Site Geometry of Q143A Human MnSOD[a]

distances		angles	
Mn−His26	2.17 (0.05)	O−Mn−Asp159	85.72 (1.17)
Mn−His74	2.19 (0.09)	O−Mn−His26	170.19 (0.22)
Mn−His163	2.15 (0.09)	O−Mn−His74	89.53 (2.71)
Mn−Asn159	2.09 (0.06)	O−Mn−His163	96.67 (0.97)
Mn−HOH	2.26 (0.04)	His163−Mn−His26	90.97 (0.30)
		His163−Mn−His74	134.28 (1.50)
		His163−Mn−His159	115.45 (0.53)
		His26−Mn−Asp159	85.87 (0.12)
		His74−Mn−Asp159	110.15 (1.05)
		His74−Mn−His26	89.12 (0.64)

[a] The bond lengths (in angstroms) and angles (in degrees) are averaged over both of the molecules that are in the asymmetric unit, and the error is given in parentheses.

RESULTS

Structure and Spectroscopy. The overall structure of Q143A human MnSOD is not significantly different from the wild-type enzyme; the root-mean-square deviation between the Cα's of the mutant and the wild type is 0.23 Å. As in the wild-type structure, the active site of this mutant is pentacoordinate about the manganese ion with three histidines, one aspartate, and one solvent molecule as ligands. In both MnSOD and FeSOD, the five ligands of the metal are arranged in a strained trigonal bipyramidal geometry; these bond lengths and angles, averaged over both molecules in the asymmetric unit for the Q143A MnSOD crystals, are listed in Table 1 and are consistent with those of other Mn- and Fe-containing SOD's (*4*, *10*, *11*, *23*). According to atomic absorption spectroscopy, the Q143A enzyme in solution had 66% of its active sites occupied by manganese in solution. The *B*-factors of the manganese and its bound solvent molecule are comparable to those of the wild-type structure, showing that in the crystals the metal contents of their active sites are also comparable. The average *B*-factor for both manganese ions and bound water molecules is 20 Å^2 for Q143A, a value that is not significantly different from those calculated in the wild-type structure [average *B*-factor for the Mn in both molecules of the asymmetric unit was 19 Å^2 and for the bound solvent molecules it was 22 Å^2 (*4*)].

While the first shell of ligands is conserved from the wild type to the Q143A mutant, two new water molecules fill the cavity created by changing the glutamine to an alanine. Each water molecule lies in nearly the same position as the Oε or Nε of the replaced glutamine (Figure 1B). The water molecule that takes the place of the nitrogen from the glutamine is about 3.0 Å from the Mn-bound water molecule and about 2.2 Å from the hydroxyl of Tyr 34, fulfilling in part the role of the glutamine in maintaining the hydrogen bond network. The second water molecule is about 2.75 Å from the first water molecule, about 2.9 Å from the Nε of Trp 123, and about 3.25 Å from the Mn-bound water molecule. The density for both novel water molecules is strong, and the average *B*-factor for each is 44 and 25 Å^2, respectively, suggesting that the water molecule that connects

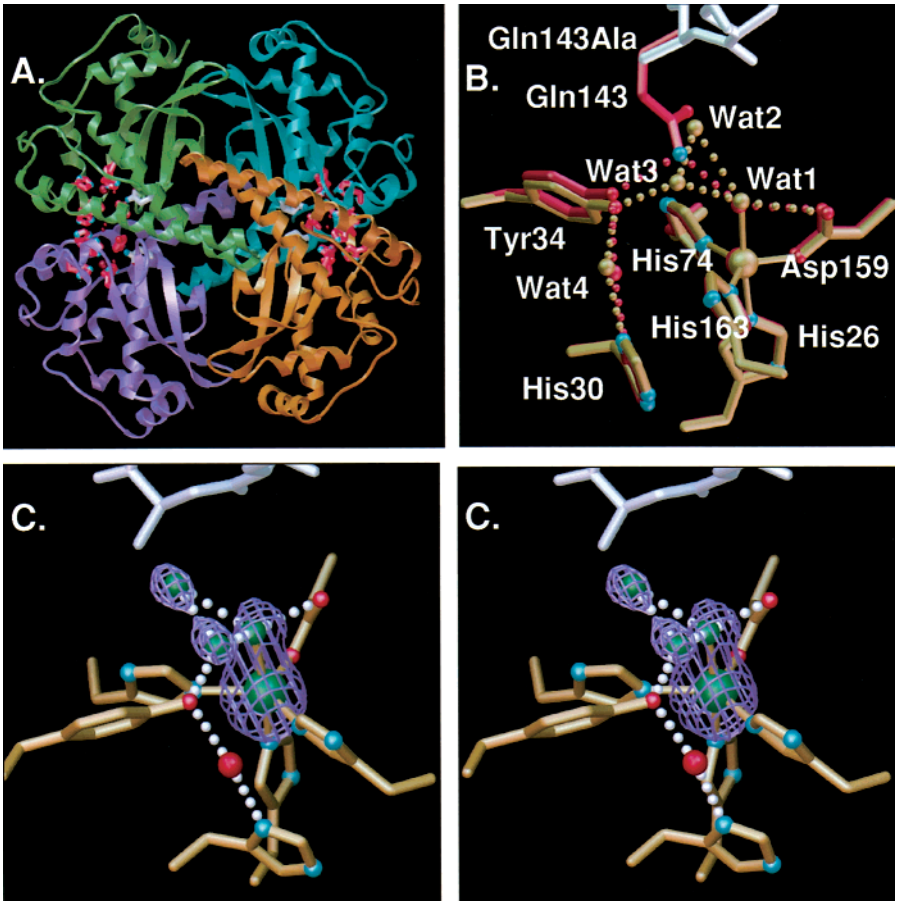

FIGURE 1: (A) Crystal structure of tetrameric human wild-type MnSOD with subunits shown in different colors (*4*). The manganese, the residues that coordinate the manganese, and the residues involved in the hydrogen bond network in the active site are pink. Glutamine 143 is white. (B) Superposition of the active-site regions from the crystal structures of the wild-type human MnSOD and the Q143A mutant. The residues from the wild-type MnSOD are pink, those from Q143A are gold, but alanine 143 is white. In the structure of Q143A, two novel water molecules (Wat2 and Wat3) fill the space left by the glutamine to alanine change and superimpose on the positions occupied by Nϵ and Oϵ of the wild-type glutamine 143. Wat1 is the manganese-bound solvent molecule. (C) Stereoview of the active site of Q143A MnSOD with an $F_o - F_c$ omit map contoured at 3σ. The three water molecules and the manganese were omitted and are green. Alanine 143 is white, and hydrogen bonds are white dots.

the Mn-bound solvent to Tyr 34, as well as the water molecule that is further from the active site, is not localized to a single position. The locations of these water molecules and the surrounding protein side chains show that the hydrogen bond network is maintained in the mutant structure, although it is not as well ordered as it is in the wild-type structure in which a well-positioned glutamine fills the same space and performs catalysis more efficiently.

Wild-type human MnSOD is purified predominantly in the Mn(III) state (*1*) and exhibits a strong absorbance in the visible range with a maximum at 480 nm ($\epsilon_{480} = 610$ M^{-1} cm^{-1}). In contrast, the visible absorption spectra of the mutants at position 143 listed in Table 2 displayed only a very weak visible absorption ($\epsilon_{480} < 30$ M^{-1} cm^{-1}) characteristic of MnSOD in the Mn(II) state (typical spectra shown in Figure 2). This was taken as evidence that, like Q143N human MnSOD (*11*), these mutants have been purified with manganese predominantly in the reduced state. Moreover, the active sites of wild-type MnSOD were about 80−90% occupied by manganese and less than 3% occupied by iron whereas mutations at position 143 increased the iron content of the mutants as determined by atomic absorption spectroscopy. For example, Q143A MnSOD had 66% manganese and 10% iron. In samples of varied iron content, the catalytic activity correlated with the manganese content, indicating that the Fe-containing mutants were inactive or had activity too low to detect.

Table 2: Values of the pH-Independent Steady-State Kinetic Constants for the Dismutation of Superoxide Catalyzed by Wild-Type Human MnSOD and Mutants at Position 143[a]

residue at position 143	k_{cat} (ms^{-1})	k_{cat}/K_m (μM^{-1} s^{-1})
Gln (wild type)[b]	40	800
Ala	0.50	3.1
Val	~0.8[c]	0.7
Asn[b]	0.30	0.82
Glu	0.32	0.63
His	0.19	5.2

[a] Stopped-flow data collected at pH 9.6 and 20 °C, except where otherwise noted. The constants for these mutants were observed to be independent of pH in the range of pH 8.0−10.5 except for Q143N which decreased with increasing pH (*11*). The standard errors were at most 15% for k_{cat}/K_m and 20% for k_{cat}. [b] From Hsieh et al. (*11*); data collected at pH 9.4 and 20 °C. [c] Because the value of K_m for this mutant was near 1 mM (larger than the K_m for the remaining enzymes of this table), we were only able to roughly estimate this constant. In this particular case, the estimated uncertainty is as great as 40%.

Catalysis. The catalyzed decay of superoxide was measured by stopped-flow spectrophotometry and pulse radiolysis from the absorbance of $O_2^{\bullet -}$ at 250 or 260 nm; Figure 3 shows typical data for Q143A MnSOD. Each of the mutants listed in Table 2 was adequately fit to Michaelis−Menten

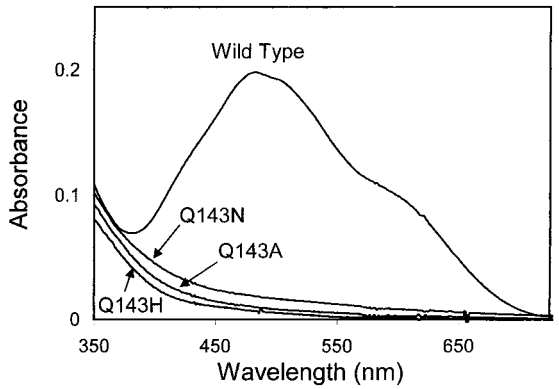

FIGURE 2: Visible absorbance spectra of wild-type human MnSOD and site-specific mutants Q143A, Q143H, and Q143N measured at pH 7.8 and 20 °C. Solutions contained 20 mM phosphate buffer and 100 μM EDTA.

FIGURE 3: Superoxide decay catalyzed by Q143A MnSOD following introduction of superoxide by pulse radiolysis at 25 °C. Data show the decrease in absorbance at 260 nm due to superoxide [ϵ = 2000 M^{-1} cm^{-1} (*26*); path length 2.0 cm]. The initial concentration of superoxide was 22 μM, and the solution contained 1.0 μM Q143A MnSOD, 2.0 mM Taps at pH 8.2, 30 mM sodium formate, and 50 μM EDTA. The solid line is a fit to a first-order decay giving a rate constant of 2.0 $\pm$ 0.1 s^{-1}.

kinetics. Values of k_{cat}/K_m and k_{cat} were quite similar for the mutants and smaller than the values for wild-type MnSOD by 2−3 orders of magnitude (Table 2). Both k_{cat} and k_{cat}/K_m for these mutants showed no pH dependence in the pH range from 8.0 to 10.5; an exception was Q143N for which these parameters decreased with increasing pH (*11*). We also prepared and carried out measurements of the mutant Q143S; it had values of k_{cat} and k_{cat}/K_m that were too small to measure accurately because of the rapid competing uncatalyzed dismutation. These results are under further investigation.

When observing the decreasing UV absorbance of superoxide itself (250−260 nm), catalysis by wild-type MnSOD exhibits a prominent phase zero-order in superoxide beginning about 2 ms after introduction of $O_2^{\bullet-}$ and characteristic of product inhibition (*1*−*3*). When observing the absorbance of the enzyme itself, the product-inhibited state of wild-type MnSOD has been associated with an absorbance at 420 nm ($\epsilon_{420} \approx 500$ M^{-1} cm^{-1}) (*2*, *13*). Both pulse radiolysis and scanning stopped-flow experiments with mutants at position 143 have detected such an absorption. In pulse radiolysis experiments, catalysis by Q143A MnSOD was accompanied by the emergence and decay of an absorbance at 420 nm (Figure 4). These data could be described by the sum of two exponentials, one for the emergence and one for the decrease of the absorbance at 420 nm with rate constants given in the legend (Figure 4). These measurements were repeated

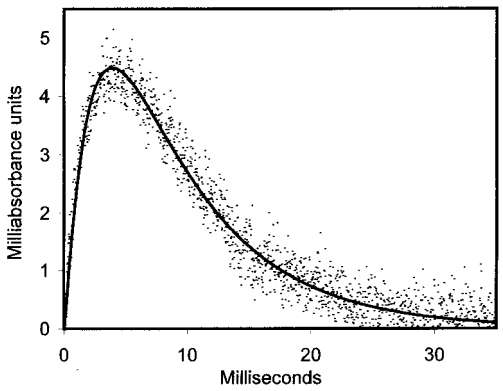

FIGURE 4: Emergence and decay of the absorbance at 420 nm (path length 2.0 cm) of Q143A MnSOD following the introduction of 13 μM superoxide by pulse radiolysis. The solution contained 90 μM Q143A MnSOD, 2.0 mM Taps, 30 mM formate, and 50 μM EDTA at pH 8.2 and 25 °C. The solid line is a fit to the sum of two exponentials giving rate constants of 447 $\pm$ 15 s^{-1} for the emergence and 125 $\pm$ 3 s^{-1} for the decay of absorbance.

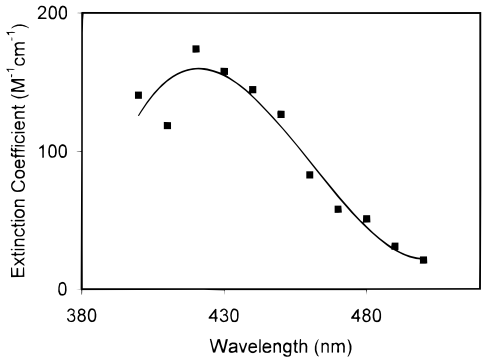

FIGURE 5: Change in extinction coefficient, ϵ (M^{-1} cm^{-1}), as a function of wavelength obtained by extrapolation of the decreasing phase of absorbance to the initial time of mixing of superoxide and Q143A MnSOD. Data such as shown in Figure 4 were measured at a series of wavelengths; each set of data was fit to the sum of two exponentials, and the fit of the decay was extrapolated to time zero. Pulse radiolysis conditions were as described in Figure 4.

at different wavelengths in the visible range, and the exponential decay was extrapolated to the initial time of mixing. The resulting plot (Figure 5) showed a maximum absorbance at 420 nm ($\epsilon_{420} \approx 160$ M^{-1} cm^{-1}) and described a spectrum for the inhibited phase. Using scanning stopped-flow spectrophotometry and mixing $O_2^{\bullet-}$ and Q143A MnSOD, we also observed spectra with a maximal absorption at 420 nm (data not shown).

Differential Scanning Calorimetry. The thermal stabilities of the wild-type and position 143 mutants were determined by differential scanning calorimetry. In general, three melting temperatures can be observed for MnSOD (*17*): a sometimes detectable but very weak transition labeled component A, a component B that is also very weak and corresponds to the thermal inactivation temperature of the wild-type enzyme (T_m 70 °C), and component C which is the main unfolding transition. The area of transition C is always greater than 95% of the total area of transitions A, B, and C. The five different residues incorporated at position 143 had profound effects on the heat stability of the enzyme (Table 3). In all cases, transitions A and B are barely detectable, and for the mutant Q143S, it was not observed. This suggests that for Q143S either transition B has a very small calorimetric

Table 3: Transition Temperatures for the Unfolding of Wild-Type Human MnSOD and Mutants at Position 143

residue at position 143	T_m (°C)
Glu	103.0
Ser	94.9
Asn[a]	90.7
Gln (wild type)[a]	88.9
His	88.9
Ala	79.8
Val	68.2

[a] From Guan et al. (*10*).

enthalpy such that it is not detectable or the two transitions B and C are superimposed. This was the case with the mutants at position 30 (*6*); an unambiguous identification of transitions A and B was not possible. However, the main unfolding transition C, which can be clearly measured, is the main determinant of conformational stability.

DISCUSSION

In the wild-type MnSOD, Gln 143 participates in an extensive hydrogen-bonded network in the active site; it forms a hydrogen bond with the manganese-bound solvent and the phenolic hydroxyl of Tyr 34. Its replacement in Q143N (*11*) and Q143A (Figure 1) alters this hydrogen-bonded chain by inserting one or two water molecules, respectively, in this network. The more conservative replacements of Gln 143 with Asn and His had almost no effect on the main thermal unfolding transition T_m; the values for Q143N (90.7 °C, Table 3) and Q143H (88.9 °C) were similar to that of wild type (88.9 °C). The small effect on T_m of His 143 is interesting since His is found at this position in cambialistic bacterial MnSODs (*24*). Replacement of Gln with both Ala (79.8 °C) and Val (68.2 °C) significantly destabilized the enzyme, presumably because the inability of these side chains to form hydrogen bonds disrupted the hydrogen bond network around position 143. In addition, Val is the most destabilizing replacement, and it also is the only replacement with a branched β-carbon. Replacement by Ser (94.9 °C) or Glu (103.0 °C) offered considerable stabilization possibly because of a reinforcement of the hydrogen-bonding network. We attempted to prepare Q143K, placing a positively charged residue at position 143; however, this mutant was too unstable to purify.

There is evidence that k_{cat} is determined at least in part by proton-transfer processes that form product H_2O_2 in MnSOD (*2*) and FeSOD (*25*). This result extends to Q143N MnSOD for which the solvent hydrogen isotope effect on k_{cat} is 1.9 (*11*). The lower values of k_{cat} in catalysis by the site-directed mutants of Table 2 compared with wild type suggest that protons cannot be as efficiently transferred to the active site despite the presence of water molecules that provide the possibility of re-forming the hydrogen-bonded network and providing a proton source and pathway. The significance of the rather similar values of k_{cat} for the mutants of Table 2 suggests that there is considerable flexibility in the residues that can sustain k_{cat}, but none of them are able to participate in product formation to the same extent as in the wild-type MnSOD. The large decrease in the values of k_{cat}/K_m for the mutants of Table 2 compared with wild type indicates substrate diffusion is not rate-determining in the mutants. The visible absorption spectra (Figure 2) of selected mutants from Table 2 show that reduced metal is prominent, whereas in the wild type the oxidized metal predominates in the purified form in the resting state. In Q143A MnSOD, the appearance of water molecules at the approximate locations of the Oϵ and Nϵ of Gln 143 of wild type, and the formation of the hydrogen-bonded network including these water molecules, was not sufficient to maintain either the catalytic activity or the redox potential of the mutant.

Table 4: Values of the Zero-Order Rate Constant $k_0/[E_o]$ Describing the Product-Inhibited Phase, and Rate Constants k_5 and k_{-5} (of Eq 2) for the Formation and Dissociation of the Product-Inhibited Complex, during the Decay of Superoxide Catalyzed by Human Wild-Type and Q143A MnSOD

enzyme	$k_0/[E_o]$ (s^{-1})	k_5 ($\mu M^{-1} s^{-1}$)[a]	k_{-5} (s^{-1})[a]
Q143A	>2000[b]	1.4	103 ± 10
wild type	500	1100	117 ± 5

[a] k_5 and k_{-5} of eq 2 were determined by least-squares fit of the catalytic scheme of McAdam et al. (*3*) to the change in absorption at 420 nm; in this fit, the values of the rate constants for the oxidation−reduction cycle of catalysis were made consistent with the experimentally observed values of k_{cat}/K_m. [b] No zero-order region of enzyme inhibition was observed with this mutant. The lower limit was estimated from the smallest zero-order decay that would have been detectable in our measurements.

Hsieh et al. (*11*) observed catalysis by human Q143N MnSOD and, based on the decay of the UV absorbance of superoxide, suggested no significant product inhibition. In fact, the observations in this report of the catalyzed decay of superoxide measured by the decrease of its UV absorbance are also consistent with no product inhibition; Figure 3 shows no evidence of a phase zero-order in superoxide during catalysis by Q143A MnSOD. However, during catalysis by these mutants, we observed the presence of a transitory absorbance at 420 nm characteristic of product inhibition, shown for Q143A in Figures 4 and 5. The absorbance of Q143A MnSOD at 420 nm gave an extinction coefficient near 160 M^{-1} cm^{-1} when extrapolated to the time of introduction of superoxide (Figure 5), although this may not represent full inhibition of the enzyme. The estimated extinction coefficient of the product-inhibited complex of wild-type MnSOD is near 500 M^{-1} cm^{-1} (*2*, *13*); wild-type MnSOD is more strongly product-inhibited than Q143A, and hence this value is probably a more accurate estimate for the inhibited complex. We calculate that at the time of maximum absorbance of Q143A in Figure 4, approximately 5−15% of the active sites are in the product-inhibited state, depending on which of the above extinction coefficients we use. Thus, although not detected as a deviation of first-order kinetics in Figure 3, there is a very small amount of product inhibition even in the mutant Q143A.

This allows us to comment on the characteristics of the product-inhibited state by comparing the very weakly inhibited mutants of MnSOD in Table 2 with wild-type human MnSOD which exhibits considerable product inhibition (*1*). The extent of inhibition is quantitated by the rate constant $k_o/[E_o]$ of the product-inhibited phase of catalysis which is zero-order in superoxide (*1*, *2*); values of $k_o/[E]$ are given in Table 4. Also included in Table 4 is an estimate of the rate constants for the formation and dissociation of the product-inhibited enzymes (k_5 and k_{-5} of eq 2) obtained from pulse radiolysis data such as shown in Figure 4. A rough estimate of these constants is obtained directly from the least-

squares fit of these data to the sum of two exponentials which gives a value of k_5 of 5×10^6 M^{-1} s^{-1} (dividing the rate constant for the emergence of the 420 nm absorption by enzyme concentration) and k_{-5} of 125 s^{-1}. These rate constants are a good approximation under the single-turnover conditions of the pulse radiolysis experiments. A more refined estimate of the rate constants for k_5 and k_{-5} was determined from a least-squares fit of the rate constants of the McAdam mechanism of MnSOD (*3*) to a more extensive set of data which included the appearance and decay of the 420 nm absorbance as in Figure 4 as well as the rate constants of the oxidation−reduction cycle. In this procedure, the rate constants describing the uninhibited oxidation and reduction cycles of catalysis were fixed at values consistent with the experimentally observed values of k_{cat}/K_m. This approach gave k_{-5} at 103 ± 10 s^{-1} for Q143A MnSOD, in agreement with the former estimate. Similar measurements on the appearance and disappearance of absorption of wild-type human MnSOD following introduction of superoxide by pulse radiolysis (data not shown) gave a value of k_{-5} of 117 s^{-1} (Table 4). This is comparable to the value of k_{-5} at 130 s^{-1} for wild-type human MnSOD at 20 °C estimated from the change in absorbance of superoxide during catalysis (*1*) and to the value of 70 s^{-1} by McAdam et al. (*3*) for *B. stearothermophilus* MnSOD at 25 °C. In contrast to these similar values of k_{-5} for Q143A and wild type, the values of k_5 differed by 3 orders of magnitude (Table 4).

The significance of the data of Table 4 is that even the very weakly active mutant Q143A shows evidence of product inhibition; moreover, the values of k_{-5} derived from the pulse radiolysis experiments are comparable in magnitude to those of the much more active and more inhibited wild-type MnSOD. Hence, Gln 143, which is necessary for maximal activity in superoxide dismutation, appears to have no role in the dissociation of the product-inhibited complex. The identity of the product-inhibited complex has not been definitively described, but it is suggested to be a side-on peroxo complex of Mn(III) at the active site (*2*). This complex would be expected to dissociate following proton transfer to form hydrogen peroxide. The results of Table 4 may indicate that proton transfer to this complex is similar in Q143A and in wild-type MnSOD. The data also suggest that the dissociation of the product-inhibited complex described by k_{-5} is not affected by the change in redox potential for the mutants at position 143. The mechanism of McAdam et al. (*3*) and the more complex mechanism of Bull et al. (*2*) for catalysis by MnSOD both show that the rate constant of the inhibited region that is zero-order in superoxide is proportional to the rate constant for the decay of the product-inhibited state, k_{-5}, as well as dependent on other steps of the catalytic, oxidation−reduction cycle. Table 4 shows a great difference in the values of k_5 for wild type and mutant; however, this difference needs to be interpreted in terms of the great differences in the other rate constants of the oxidation−reduction cycle. That is, the rate of appearance of inhibited complex will also depend on k_3 of eq 2 which we have not determined. It is apparent that for Q143A MnSOD the overall extent of product inhibition is less because the rate constants for the oxidation−reduction cycle (k_1 through k_4) and k_5 are less, not because the rate of dissociation of the inhibited complex is greater. These considerations will be significant in determining the properties of the product inhibition in human MnSOD and in the design of variants of MnSOD for gene therapy research which are strongly catalytic but weakly inhibited.

ACKNOWLEDGMENT

It is a pleasure to acknowledge the assistance of Kristi Totten and Harold Frey. We are grateful to Sudip S. Parikh and Douglas S. Daniels for help with data collection.

REFERENCES

1. Hsu, J.-L., Hsieh, Y., Tu, C. K., O'Connor, D., Nick, H. S., and Silverman, D. N. (1996) *J. Biol. Chem. 271*, 17687−17691.
2. Bull, C., Niederhoffer, E. C., Yoshida, T., and Fee, J. A. (1991) *J. Am. Chem. Soc. 113*, 4069−4076.
3. McAdam, M. E., Fox, R. A., Lavelle, F., and Fielden, E. M. (1977) *Biochem. J. 165*, 71−79.
4. Borgstahl, G. E. O., Parge, H. E., Hickey, M. J., Beyer, W. F., Hallewell, R. A., and Tainer, J. A. (1992) *Cell 71*, 107−118.
5. Borders, C. L., Bjerrum, M. J., Schirmer, M. A., and Oliver, S. G. (1988) *Biochemistry 37*, 11323−11331.
6. Ramilo, C. A., Leveque, V., Guan, Y., Lepock, J. R., Tainer, J. A., Nick, H. S., and Silverman, D. N. (1999) *J. Biol. Chem. 274*, 27711−27716.
7. Hunter, T., Ikebukuro, K., Bannister, W. H., Bannister, J. V., and Hunter, G. J. (1997) *Biochemistry 36*, 4925−4933.
8. Sorkin, D. L., Duong, D. K., and Miller, A.-F. (1997) *Biochemistry 36*, 8202−8208.
9. Whittaker, M. M., and Whittaker, J. W. (1997) *Biochemistry 36*, 8923−8931.
10. Guan, Y., Hickey, M. J., Borgstahl, G. E. O., Hallewell, R. A., Lepock, J. R., O'Connor, D., Hsieh, Y., Nick, H. S., Silverman, D. N., and Tainer, J. A. (1998) *Biochemistry 37*, 4722−4730.
11. Hsieh, Y., Guan, Y., Tu, C. K., Bratt, P. J., Angerhofer, A., Lepock, J. R., Hickey, M. J., Tainer, J. A., Nick, H. S., and Silverman, D. N. (1998) *Biochemistry 37*, 4731−4739.
12. Cabelli, D. E., Guan, Y., Leveque, V., Hearn, A. S., Tainer, J. A., Nick, H. S., and Silverman, D. N. (1999) *Biochemistry 38*, 11686−11692.
13. Hearn, A. S., Tu, C. K., Nick, H. S., and Silverman, D. N. (1999) *J. Biol. Chem. 274*, 24457−24460.
14. Beck, Y., Oren, R., Amit, B., Levanon, A., Gorecki, M., and Hartman, A. J. (1987) *Nucleic Acids Res. 15*, 9076.
15. Beck, B. A., Bartfield, D., Yavin, Z., Levanon, A., Gorecki, M., and Hartman, J. R. (1988) *BioTechnology 6*, 930−935.
16. McRee, D. E. (1992) *J. Mol. Graphics 10*, 44−47.
17. Borgstahl, G. E. O., Parge, H. E., Hickey, M. J., Beyer, W. F., Hallewell, R. A., and Tainer, J. A. (1996) *Biochemistry 35*, 4287−4297.
18. Sturtevant, J. M. (1987) *Annu. Rev. Phys. Chem. 38*, 463−488.
19. McClune, G. J., and Fee, J. A. (1978) *Biophys. J. 24*, 65−69.
20. Valentine, J. S., and Curtis, A. B. (1975) *J. Am. Chem. Soc. 97*, 224−226.
21. Marklund, S. (1976) *J. Biol. Chem. 251*, 7504−7507.
22. Schwarz, H. A. (1981) *J. Chem. Educ. 58*, 101−105.
23. Lah, M. S., Dixon, M. M., Pattridge, K. A., Stallings, W. C., Fee, J. A., and Ludwig, M. L. (1995) *Biochemistry 34*, 1646−1660.
24. Jackson, S. M. J., and Cooper, J. B. (1998) *Biometals 11*, 159−173.
25. Bull, C., and Fee, J. A. (1985) *J. Am. Chem. Soc. 107*, 3295−3304.
26. Rabani, J., and Nielson, S. O. (1969) *J. Phys. Chem. 73*, 3736−3744.

BI9929958